OPTICA

Reducing the noise of fiber supercontinuum sources to its limits by exploiting cascaded soliton and wave breaking nonlinear dynamics

Benoît Sierro,* Pascal Hänzi, Dirk Spangenberg, Anupamaa Rampur, and Alexander M. Heidt

Institute of Applied Physics, University of Bern, Sidlerstrasse 5, 3012 Bern, Switzerland
Corresponding author: benoit.sierro@unibe.ch

Received 7 December 2021; revised 16 February 2022; accepted 20 February 2022; published 23 March 2022

The low-noise and phase-coherent nonlinear transformation of a narrowband laser into a broadband supercontinuum (SC) in an optical fiber forms the basis of extremely precise applications ranging from optical frequency comb technology to ultrafast photonics and biomedical imaging. A major challenge of this process is the avoidance of incoherent nonlinear effects that amplify random quantum noise, requiring careful birefringence and dispersion engineering of the fiber. However, fundamental trade-offs exist between working in normal or anomalous dispersion regimes. Here, we combine the benefits of nonlinear dynamics in both regimes by cascading soliton compression and optical wave breaking in a hybrid fiber, formed by joining two widely available, commercial, polarization-maintaining step-index fibers exhibiting anomalous and all-normal dispersion, respectively. We experimentally demonstrate that this hybrid approach results in an ultra-low-noise fiber SC source covering the 930–2130 nm range with phase coherence near unity, spectrally resolved relative intensity noise (RIN) as low as 0.05%, and averaging 0.1% over a bandwidth of 750 nm, approaching the theoretical limits close to the pump laser noise. This corresponds to a doubling of the generated spectral bandwidth and a decrease of RIN by up to 1 order of magnitude compared to direct pumping of the individual fibers, where modulational polarization instabilities play a limiting role. Owing to its simplicity and its scalability to high repetition rates, our hybrid scheme is readily applicable to various laser platforms and could enhance the performance of applications such as hyperspectral nonlinear microscopy, coherent optical communications, and photonic signal processing.

https://doi.org/10.1364/OPTICA.450505

1. INTRODUCTION

A major current challenge in nonlinear optics is the development of ultra-low noise broadband coherent supercontinuum (SC) light sources. Equipped with the brightness of a laser and ultra-broad spectral bandwidths, SC sources based on specialty optical fibers are today an indispensable tool in many scientific and industrial processes [1,2]. However, for many applications in advanced spectroscopy, microscopy, and ultrafast photonics, the noise of current SC sources has become the predominating factor limiting acquisition speed, sensitivity, or resolution [3]. Significant research efforts are also directed toward understanding the fundamental noise limits of the involved nonlinear spectral broadening dynamics, with continued interest in the development of optical frequency comb technology not only for metrology and spectroscopy [4,5] but increasingly also for emerging applications in coherent optical communications, microwave photonics, and photonic signal processing [6–8], where ultra-low amplitude- and phase-noise performance is an essential prerequisite.

The predominating noise source during the nonlinear transformation of a narrowband input into a broadband SC spectrum in an optical fiber is the amplification of random quantum fluctuations by incoherent nonlinear effects, which either have a scalar character, such as modulation instability or stimulated Raman scattering [9–11], or a vectorial nature emerging from a coupling of the two orthogonal eigenmodes of the fiber, such as polarization modulation instability (PMI) [12,13]. The occurrence and strength of these processes depend critically on the dispersion and birefringence engineering of the fiber, as well as on the characteristics of the input pulse [3]. Therefore, a considerable effort has been directed toward identifying fiber designs that favor highly coherent spectral broadening dynamics.

Typically, there is a trade-off to be considered when engineering the dispersion landscape of nonlinear fibers. On one hand, recent advances in specialty optical fiber design and fabrication have facilitated the emergence of a new generation of highly birefringent, polarization-maintaining (PM) all-normal dispersion (ANDi) fibers, which are designed to suppress both scalar and vectorial noise-amplifying incoherent nonlinear effects under sub-picosecond pumping [2,3]. As additional benefit, the nonlinear dynamics are dominated by optical wave breaking (OWB), which is capable of simultaneously delivering low noise, octave-spanning bandwidth, superb spectral flatness, high spectral power densities, and single-cycle temporal waveform support [14]. This new class of SC sources has driven recent advancements of the state-of-the-art in several applications, which so far were either not able to use or were limited by conventional fiber SC sources due to their noise or complex spectra and pulse shapes, e.g., in hyperspectral and multimodal imaging, near-field optical microscopy, optical coherence tomography at the shot-noise limit, and ultrafast photonics [15–21].

On the other hand, SC noise is reduced, and coherence is improved by shorter input pulse durations in any fiber design [9,22]. Here, anomalous dispersion fibers have a clear advantage as they benefit from an initial stage of soliton compression dynamics, which shorten the injected pulse to a fraction of its initial duration and increase its peak power by up to 1 order of magnitude before the actual spectral broadening dynamics set in [23]. Hence, conventional SC sources require significantly lower input peak power than ANDi SC sources for the generation of equal spectral bandwidths and, consequently, are often the only choice for the nonlinear spectral broadening of lasers with repetition rates of hundreds of megahertz or gigahertz, where the peak power per pulse is limited. Unfortunately, the subsequent soliton fission dynamics produce rather complex spectral and temporal profiles, and the anomalous dispersion environment provides strong amplification for incoherent nonlinear processes [3].

Inspired by early works with dispersion-flattened and dispersion-decreasing fibers [24,25], in this paper, we combine the benefits of nonlinear dynamics in both dispersion regimes, i.e., soliton compression and OWB, resulting in an ultra-low noise and highly coherent fiber SC source covering the 930–2130 nm range with a spectrally resolved relative intensity noise (RIN) as low as 0.05% and averaging 0.1% over a bandwidth of 750 nm. The source is based on a standard ultrafast Er:fiber laser seeding cascaded nonlinear dynamics in two discrete, widely available commercial PM step-index fibers. The individual fibers exhibit anomalous and all-normal chromatic dispersion at the pump wavelength, respectively, and are joined together by a low-loss fusion splice to form a hybrid fiber. We show that this hybrid approach not only doubles the generated spectral bandwidth but also decreases the RIN by up to 1 order of magnitude compared to direct pumping of the individual fibers. While our measurements reveal that PMI instabilities set a lower limit to the RIN of the directly pumped ANDi SC source, we identify a novel noise suppression mechanism in the hybrid fiber such that the SC noise approaches the theoretical limit determined by the noise and pulse shape of the pump laser.

2. HYBRID FIBER PREPARATION

The fibers used in this work are two commercial PM step-index fibers produced by Coherent-Nufern, namely PM1550-XP and PM2000D, which exhibit anomalous and all-normal chromatic dispersion at the pump wavelength of 1560 nm, respectively, as shown in Fig. 1 [26]. PM1550-XP has a core-diameter of 8.5 μm and numerical aperture (NA) of 0.125, resulting in a zero-dispersion wavelength of 1.34 μm and dispersion parameter $D = 18$ ps/(nm km) at 1560 nm. In contrast, the small 2.1 μm diameter core, high NA of 0.37, and highly germanium (Ge)-doped core material composition of PM2000D were specifically designed to exhibit flat and normal dispersion over the entire near-IR spectral region, with $D = -46$ ps/(nm km) at 1560 nm. Both fibers are PANDA-type PM fibers, with birefringence values at the pump wavelength of 3×10^{-4} given by the manufacturer for PM1550-XP, and 2×10^{-5} measured in-house for PM2000D.

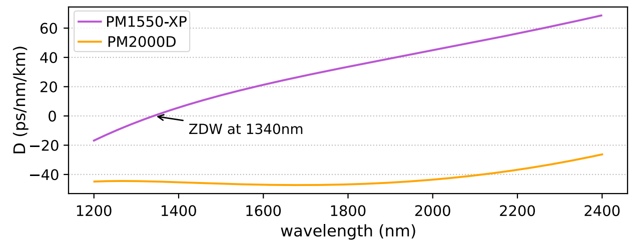

Fig. 1. Measured chromatic dispersion profiles of PM1550-XP and PM2000D fibers used to form the hybrid fiber in this study.

In order to exploit cascaded nonlinear dynamics in both fibers, a low-loss fusion splice is an essential requirement. However, losses in the order of 4 dB are to be expected with a standard splicing recipe due to the large core diameter and NA mismatch. Better results can be obtained with the thermally expanding core (TEC) technique [27]. Owing to the high Ge content of the PM2000D core material, long arc durations lead to thermal diffusion of Ge from the core to the cladding region, which gradually increases the mode field diameter in the hot zone and, thus, reduces the splice loss. By monitoring the transmission of a 1550 nm continuous-wave laser in real-time during the splice, we reach a minimum splice loss of 0.7 dB (85% transmission) with an arc time of 14 s. The splice is executed simply by modifying the arc duration of the standard PM single-mode program of a Fujikura FSM45+ fusion splicer and using auto-alignment of the polarization axes.

3. SOLITON PRE-COMPRESSION

After the splice, the hybrid fiber is cleaved such that it consists of a 6.2 cm length of PM1550-XP at the input followed by 20 cm of PM2000D, where in the former soliton compression and in the latter OWB dynamics are exploited. Hence, the length of PM1550-XP is of particular importance in our approach and was carefully optimized using the numerical pulse propagation simulations and experimental time-domain ptychography (TDP) measurements summarized in Fig. 2 [28,29]. In the fiber, the 110 fs, 32 kW, 40 MHz input pulse supplied by the Er:fiber laser forms a soliton of order $N = 4.3$ that temporally compresses until soliton fission around 6.5 cm breaks it up into its fundamental constituents. The optimized fiber length is chosen such that the resulting pulse is as short as possible while avoiding soliton fission. Figures 2(b) and 2(d) show the simulated compressed pulse with 15.9 fs full width at half-maximum (FWHM) and the corresponding spectrum, respectively, using the final fiber length of 6.2 cm. Both results are in excellent agreement with the experimental TDP measurements done using a separately prepared PM1550-XP fiber of equal length. The input pulses are, therefore, compressed by a factor of 7 while the peak power increases by a factor of about 5.3 to 170 kW, with the remaining energy distributed in a low-level pedestal typical of soliton compression. We also note that increasing the fiber length beyond the point of soliton fission does not significantly increase the spectral bandwidth in this case, as shown in Fig. 2(c), apart from the formation of a dispersive wave (DW) around 1 μm wavelength.

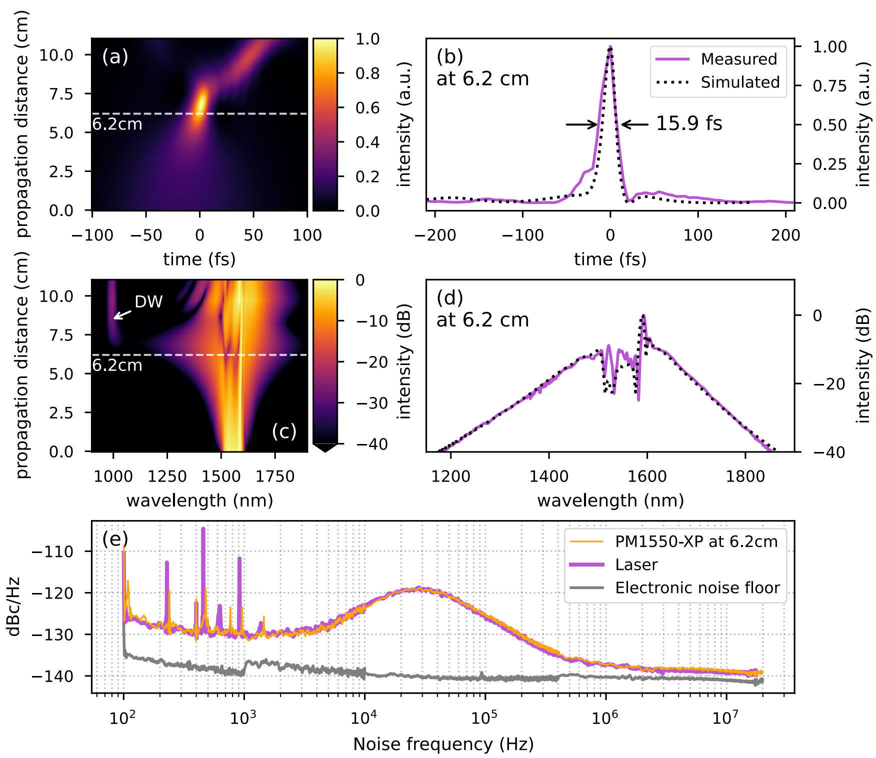

Fig. 2. Soliton compression in the PM1550-XP fiber pumped with 110 fs, 32 kW input pulses. (a) Simulated temporal intensity profile as function of propagation distance. (b) Simulated (dashed) and measured (solid) pulse shape at 6.2 cm. The measured pulse is recorded after propagating through dispersive elements (thin lens and half-wave plate) and, therefore, slightly longer (20.6 fs). (c) Simulated spectral evolution; DW, dispersive wave. (d) Simulated (dotted) and measured (solid) spectra at 6.2 cm. (e) Frequency resolved noise measurements of the injected pump and the compressed soliton pulse trains.

We perform RIN measurements in order to analyze the stability of the compressed 16 fs pulse train. Our methodology, applied for all measurements presented in this paper, is based on low-bandwidth photodetection, low-pass filtering, and extraction of the noise power spectral density (PSD) at baseband frequencies in the range from 100 Hz up to half of the repetition rate $f_{rep}/2 = 20$ MHz with an electronic spectrum analyzer (ESA). The measurement bandwidth is limited to $f_{rep}/2$ because it corresponds to the Nyquist frequency marking the fastest shot-to-shot intensity modulation that can occur in a pulse train. The approach is routinely used for the characterization of ultrafast laser sources and yields a complete measurement of the intensity noise if it extends to $f_{rep}/2$, as is done in our work [30,31] (see Supplement 1 for further details). Figure 2(e) shows that the noise power spectra of the soliton-compressed pulses and the driving Er:fiber are indistinguishable, and the integrated RIN is 0.06% in both cases. Hence, the substantial temporal compression and peak power amplification are obtained without incurring any noise penalty. The broad peak in the noise spectrum at mid-range frequencies between 10 kHz and 100 kHz stems from intracavity dynamics of the Er:fiber oscillator, while the sharp peaks at low frequencies can be traced to power supplies as well as vibrationally and acoustically induced noise from the laboratory environment, which can slightly change between measurements. We note that spectrally resolved RIN measurements of the soliton-compressed pulses reveal locally increased RIN up to 0.52% (see Supplement 1, Figure S2), but this is less relevant for our purposes since spectral filtering also modifies the temporal characteristics of the pulse.

4. SUPERCONTINUUM GENERATION IN THE HYBRID FIBER

A. Enhancement of Optical Wave Breaking

In the normal dispersion regime provided by the ANDi fiber, the initial nonlinear spectral broadening dynamics are dominated by self-phase modulation (SPM) followed by OWB redistributing energy from the spectral center to the wings and smoothing the spectrum [14]. Both processes are known to provide low-noise and coherent broadening of the input pulse spectrum for our pump pulse parameters [22]. The fiber length over which these dynamics occur depends on duration T_0 and peak power P_0 of the injected pulse, $L_{OWB} \propto T_0/\sqrt{P_0}$, while the obtainable spectral bandwidth is independent of T_0 but scales approximately with $\sqrt{P_0}$ [14]. Since the pre-compressed soliton enters the ANDi fiber with much shorter pulse duration and higher peak power than the original pulse supplied by the Er:fiber laser, we expect faster nonlinear dynamics and broader SC bandwidth generated in the hybrid fiber when compared to the directly pumped, stand-alone ANDi fiber.

Figure 3 compares the measured SC spectra generated in the hybrid fiber and the directly pumped ANDi fiber. Both measurements were obtained with a coupled pump peak power of 32 kW supplied by a 110 fs Er:fiber laser at 40 MHz repetition rate and with similar overall fiber lengths. The hybrid approach increases the generated −30 dB spectral bandwidth from 76 THz to 183 THz by a factor of $2.4 \simeq \sqrt{5.3}$, which agrees well with the theoretically expected scaling of the SC bandwidth with $\sqrt{P_0}$. The hybrid fiber SC covers the range 930–2130 nm while maintaining the typical smooth shape of a SC generated predominantly by OWB. The spectral modulation around the pump wavelength,

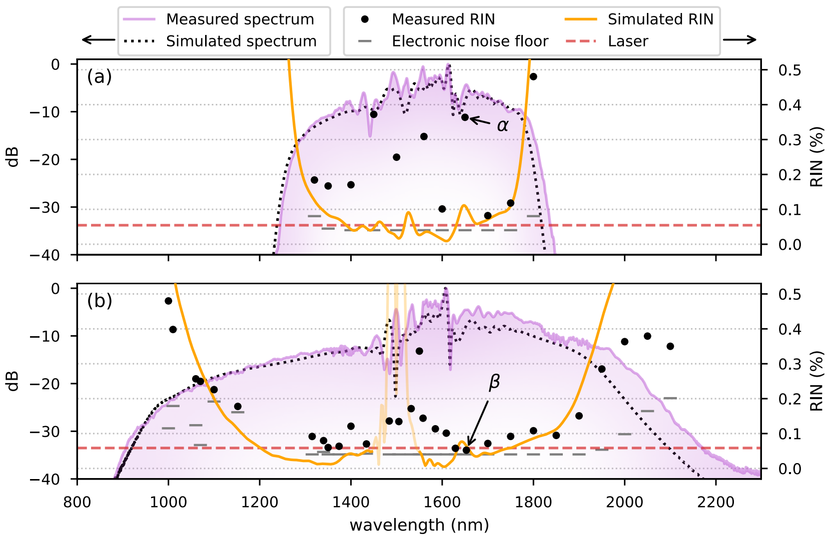

Fig. 3. Supercontinuum spectra and spectrally resolved RIN in (a) directly pumped ANDi fiber and (b) hybrid fiber for equal pumping conditions and similar fiber lengths. Left scale, measured (solid) and simulated (dotted) spectra; right scale, spectrally resolved measured RIN (dots) with corresponding electronic noise floor (-) and simulated values using scalar generalized nonlinear Schrödinger equation (GNLSE) simulations (solid yellow). The RIN of the pump laser is indicated by a red dashed line. Detailed noise frequency spectra of the RIN measurements at 1650 nm, marked α and β, are shown in Fig. 4.

observed in both fibers, can be traced back to low-level temporal sub-structures of the pump pulses emitted by the Er:fiber laser [32].

Both spectra can be reproduced very well with numerical simulations based on the generalized nonlinear Schrödinger equation (GNLSE), also shown in Fig. 3. The full simulated SC generation dynamics are visualized in Supplement 1, Fig. S5, and they confirm that the coherent OWB dynamics are enhanced and develop significantly faster in the hybrid fiber. L_{OWB} is reduced from 1.7 cm in the directly pumped ANDi fiber to only 0.1 cm in the hybrid fiber. In the following sections, we will show that these enhanced and faster coherent dynamics are the underlying physical reason for the lower noise level of the hybrid SC.

B. Reduction of Relative Intensity Noise

The spectrally resolved RIN of both SC is measured by isolating 20 nm sections of the respective spectrum with variable bandpass filters and using an ESA-based detection system sensitive to amplitude and polarization state fluctuations (see Supplement 1 for further details on the experimental procedures). The results are displayed in Fig. 3. We note that both spectral bandpass and polarization filters are important to fully characterize the SC stability. As the intensity noise of SC sources is typically anti-correlated across the spectrum [33,34], omitting these filters conceals the noise features discussed below by averaging fluctuations of anti-correlated portions of the spectrum leading to lower apparent RIN values. For this reason, our measurements are not directly comparable to studies that did not implement this spectral and polarization selectivity.

For each measured RIN value in Fig. 3, the electronic noise floor of the detection system is also displayed so that it can be easily determined whether the detected fluctuations truly stem from the SC pulse train or are limited by the noise of the measurement apparatus. We obtain a typical electronic noise floor of 0.04% RIN (or −140 dBc/Hz at high Fourier frequencies). This is higher than typically used for ultrafast laser characterization because we tuned the system not for high sensitivity at the peak wavelength but for providing a similar noise floor over as much spectral bandwidth and signal levels as possible. Nevertheless, in most cases, the electronic noise floor is sufficiently low to fully resolve the SC noise. We also compare the measured RIN levels to corresponding values retrieved from the scalar GNLSE simulations including quantum noise and technical pump laser fluctuations [35].

Surprisingly, the SC generated in the directly pumped PM2000D ANDi fiber exhibits elevated noise levels especially in the central section of the spectrum between 1400 nm and 1700 nm, where RIN values up to 0.4% are detected. While this is in range with the lowest RIN values reported to date for PM-ANDi SC sources [36], in our case, it corresponds to an order-of-magnitude amplification of the pump laser noise, which is unexpected for this fiber design. Importantly, the measured noise levels in the spectral center cannot be reproduced using scalar GNLSE simulations, which predict much lower RIN on the level of the pump laser noise. However, below 1400 nm and particularly above 1700 nm, the simulations model the measured noise evolution more accurately and also reproduce well the increasing RIN on the spectral edges due to the effect of laser peak power fluctuations on the SC bandwidth. This variation in simulation accuracy over the spectral range points toward the presence of incoherent nonlinearities with vectorial nature in the central part of the spectrum since noise amplification emerging from the nonlinear coupling of polarization eigenmodes is ignored in the scalar numerical model. Indeed, a more detailed analysis provided in Section 4.C identifies PMI as the origin of the elevated RIN.

In contrast, the intensity noise of the SC generated in the hybrid fiber is significantly lower and in general exhibits an exceptionally low variation with wavelength. The RIN follows very closely the values predicted by the scalar GNLSE simulations and remains mostly confined between 0.05% and 0.2% in the range 1150–1900 nm, with an average value of approximately 0.1%. This is quite remarkable when compared to SC generated under very similar pumping conditions in the anomalous dispersion region of a fiber, where the intensity noise varies over at least 2 orders of magnitude and reaches several percent [33]. The RIN measured

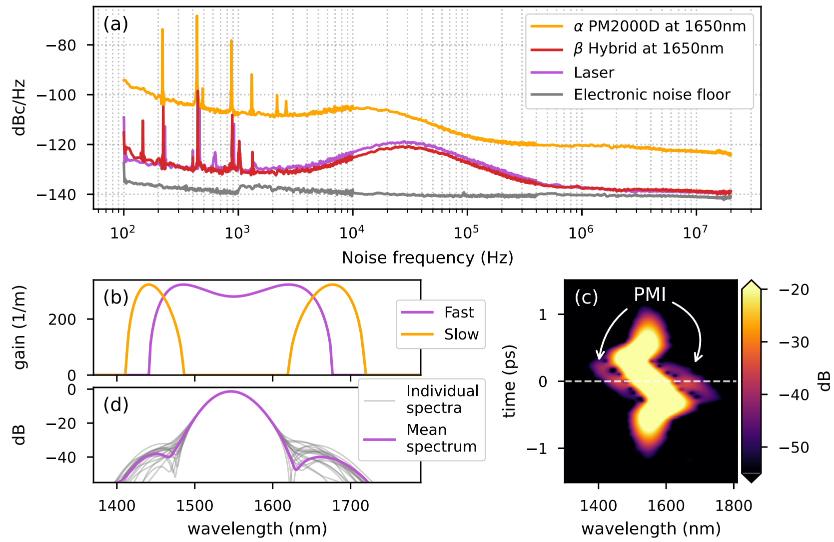

Fig. 4. (a) Detailed noise frequency spectra of the RIN measurements at 1650 nm, marked α and β in Fig. 3, compared to the pump laser. (b) Analytically calculated PMI gain in PM2000D fiber assuming a 30 kW peak power pulse propagating on slow and fast axis, respectively. (c) Simulated fast axis spectrogram of a 500 fs, 30 kW pulse after 3 cm propagation in PM2000D injected into the slow axis. (d) Spectral slice through the spectrogram in (c) at $t = 0$ for multiple simulations with random noise seeds (gray) and corresponding mean (purple).

in our experiments is also up to 1 order of magnitude lower than previously reported values obtained from stand-alone ANDi SC sources [36–38]. Higher noise only occurs at the spectral edges and in the vicinity of sharp spectral features, where small spectral shifts induced by peak power fluctuations lead to a relatively large change in SC signal. The exact spectral position of these features is hard to simulate since they sensitively depend on low-level temporal sub-structures of the input pulse interfering with spectral components generated by SPM [32]. Hence, in Fig. 3(b), the simulated RIN is faded around 1500 nm where the agreement of simulated and measured SC spectrum is less accurate. The intensity noise around these features is not linked to quantum noise amplification by incoherent nonlinearities but simply arises from the sensitivity of coherent dynamics to the input pulse parameters. Significant additional noise reduction can, therefore, only be achieved by improving the noise characteristics and the pulse shape of the pump laser.

C. Suppression of Polarization Modulation Instability

A significant advantage of the noise detection in the frequency domain over the histogram-based statistical analysis of time-domain photodiode traces in recent work [36,38] is the availability of a full noise frequency spectrum for every measured RIN value, which can be used to identify the underlying noise amplification mechanisms. We illustrate this for the RIN measurements recorded at 1650 nm, which are marked α and β in Fig. 3 and result in integrated RIN of 0.38% and 0.05% for stand-alone ANDi and hybrid fiber SC, respectively. The detailed noise spectra for these two measurements are displayed in Fig. 4(a) and are compared directly to the pump laser. The noise spectrum of the stand-alone ANDi SC is shifted upward by about 20 dB with respect to the pump due to the dominance of excess white noise, which is a characteristic signature of quantum noise amplification [10]. This unambiguously confirms the presence of incoherent nonlinear dynamics, which have to be of vectorial nature since they cannot be reproduced by scalar simulations, as discussed above. In contrast, these nonlinearities are suppressed in the hybrid fiber, which even exhibits slightly lower noise than the pump laser in the mid-range frequencies between 1 kHz and 1 MHz.

Figure 4(b) identifies PMI as the origin of this nonlinear noise amplification in the stand-alone PM2000D ANDi fiber, showing that the analytically calculated PMI gain bands [39] for our experimental conditions overlap exactly with the 1400–1700 nm spectral region where the measurements in Fig. 3(a) detect elevated RIN values. In order to illustrate how this PMI gain leads to pulse-to-pulse intensity fluctuations of the generated SC, we conduct vectorial GNLSE simulations taking into account the coherent coupling of the two polarization eigenmodes [40]. Additionally, we increase the input pulse duration to 500 fs, which enhances the visibility of the incoherent PMI dynamics by slowing down the coherent wave breaking process. The simulated spectrogram in Fig. 4(c) shows clear signatures of PMI after only 3 cm of propagation in the form of two sidebands being generated at spectro-temporal positions outside of the main pulse. As these sidebands remain unseeded, random quantum fluctuations serve as the seed and are amplified to become significant. Taking a slice through the spectrogram at $t = 0$ and repeating the simulations several times clearly shows the random amplitude fluctuations introduced by PMI at spectral positions corresponding very well to the analytically calculated PMI gain bands [compare Figs. 4(b) and 4(d)]. While we consider pure slow-axis pumping in this case, in reality we expect a blend of fast- and slow-axis dynamics as we also observe linear coupling of the polarization states in the PM2000D fiber reducing the polarization extinction ratio (PER) from >30 dB at the input to about 15 dB at the output, even at low power.

Why does PMI occur in the stand-alone ANDi fiber but is suppressed in the hybrid fiber? The underlying mechanism for this noise reduction relies on cascaded nonlinear dynamics. First, the pulse duration is shortened by soliton compression in the anomalous dispersion fiber, which subsequently enhances OWB and suppresses PMI in the ANDi fiber. Physically this can be understood by considering the characteristic length scales of the

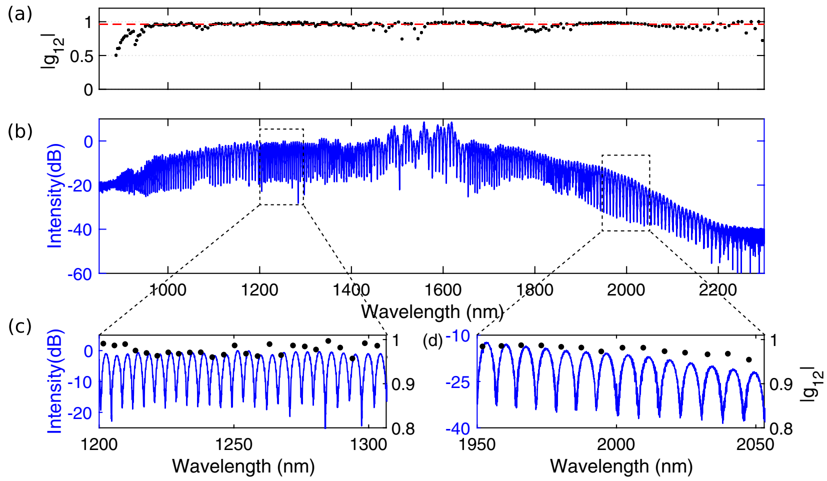

Fig. 5. Experimental phase coherence measurements of the SC generated in the hybrid fiber using spectral interferometry. (a) Magnitude of first-order coherence determined according to Eq. (1). The red dashed line indicates the spectrally averaged coherence of $\langle|g_{12}|\rangle = 0.96$. (b) Spectral interference measurement showing high extinction fringes over the entire SC bandwidth. (c), (d) Magnified views of interference fringes and coherence around 1250 nm and 2000 nm.

coherent OWB and the incoherent PMI dynamics and noting that the process with the shortest length scale plays the dominant role [39]. In the case of the stand-alone ANDi fiber, the OWB length $L_{\mathrm{OWB}} = 1.7$ cm is shorter but comparable to the PMI length $L_{\mathrm{PMI}} = 5.3$ cm, indicating a certain balance between the two processes that allows PMI to amplify noise from the shot-noise level. In the hybrid fiber, two factors suppress PMI. First, the higher birefringence and anomalous dispersion of the PM1550-XP fiber completely suppress PMI during the soliton pre-compression phase for slow-axis pumping (Supplement 1, Figure S3). Second, the pre-compressed soliton enters the ANDi fiber with much shorter duration and higher peak power than the original pulse, leading to a significant enhancement of the OWB dynamics as evident by a 17× reduction of L_{OWB} to only 0.1 cm (Supplement 1, Fig. S5). PMI, on the other hand, is independent of pulse duration and less influenced by the soliton pre-compression [39], resulting in a clear dominance of the coherent OWB dynamics. The short L_{OWB} is associated with an accelerated spectro-temporal transformation of the pulse by SPM and OWB followed by a fast drop in peak power due to dispersive stretching, which in combination prevent the accumulative buildup of noise by constantly shifting the spectro-temporal positions of the PMI gain peaks. These dynamics are very similar to the suppression of scalar incoherent Raman and four-wave mixing processes in ANDi fibers at short pulse durations discussed in detail in [22].

D. Phase Coherence

The dominance of the inherently phase-coherent processes of SPM, soliton compression, and OWB during nonlinear spectral broadening suggests that the SC generated in the hybrid fiber should also exhibit excellent phase stability. We experimentally quantify the phase fluctuations using a free-space asymmetric Michelson interferometer (see Supplement 1 for details on the experimental setup). One arm of the device is set to provide a delay with respect to the other arm corresponding to the pulse repetition period, such that two subsequent SC pulses interfere with each other. The signal is detected with an optical spectrum analyzer (OSA), where spectral interference fringes appear if the SC pulse train is phase-stable over time intervals exceeding the OSA sweep time [41]. A single sweep lasts several seconds and, thus, records the ensemble average of $> 10^8$ interference events, such that the magnitude of the degree of first-order coherence as a function of wavelength becomes measurable as [42]

$$|g_{12}(\lambda)| = \frac{V(\lambda)[I_1(\lambda) + I_2(\lambda)]}{2[I_1(\lambda)I_2(\lambda)]^{1/2}}, \tag{1}$$

where $I_1(\lambda)$ and $I_2(\lambda)$ are the measured light intensities in each arm of the interferometer and $V(\lambda)$ is the fringe visibility given by the maximum and minimum fringe intensity, $V(\lambda) = [I_{\max}(\lambda) - I_{\min}(\lambda)]/[I_{\max}(\lambda) + I_{\min}(\lambda)]$. Equation (1) is equal to the expression routinely used in numerical studies, $|g_{12}| = \langle E_1^* E_2\rangle/[\langle|E_1|^2\rangle\langle|E_2|^2\rangle]^{1/2}$, with the spectral field envelopes $E_1(\lambda)$, $E_2(\lambda)$ and ensemble average $\langle.\rangle$, but expressed in experimentally accessible variables. Note that the calculation of $|g_{12}(\lambda)|$ accounts for differences in the interfering intensities, which in practice are difficult to equalize exactly in broadband measurements, and therefore represents a better figure of merit for coherence than the visibility $V(\lambda)$ itself. The fringe spacing, and hence the spectral resolution of the coherence measurement, can be chosen by fine-tuning the temporal delay between the interfering pulses. It is well known that the value of $|g_{12}(\lambda)|$ is primarily sensitive to phase fluctuations and only to a much lesser extend to intensity noise [9,43], such that it provides a convenient, broadband, self-referenced, and high resolution measure of phase stability complementary to the RIN characterizations performed above.

Figure 5 confirms the excellent phase stability of the generated SC, evident from high contrast interference fringes with visibility in the order of 20 dB measured over the entire bandwidth of the hybrid fiber SC. $|g_{12}(\lambda)|$ is near unity for the majority of the bandwidth, as exemplary highlighted in the magnified views of Figs. 5(c) and 5(d). The coherence averaged over the full 900–2200 nm bandwidth is calculated to $\langle|g_{12}|\rangle = \int |g_{12}(\lambda)|I(\lambda)\mathrm{d}\lambda / \int I(\lambda)\mathrm{d}\lambda = 0.96$. This ranks among the highest experimentally confirmed magnitude and uniformity of $|g_{12}(\lambda)|$ for fiber- and waveguide-based SC sources to date [44–49]. Slightly degraded coherence is only detected at the spectral edges and around the sharp spectral features near the pump wavelength, coinciding with the regions of increased RIN in Fig. 3 whose origin was already discussed in Section 4.B. Near 1800 nm, the coherence measurement is disturbed by water vapor absorption lines preventing accurate extraction of visibility and intensities. Using our experimentally determined value of $\langle|g_{12}|\rangle$ and the results of previously published numerical studies [35], we can assign a median shot-to-shot timing jitter $\delta t < 0.5$ fs to the pulse train emitted by the hybrid SC source, revealing stability down to a small fraction of an optical cycle.

5. CONCLUSION

In this work, we introduce a novel approach for avoiding nonlinear noise amplification during SC generation and, thus, provide a solution for a long-standing challenge of nonlinear fiber optics. We show that cascading soliton compression and OWB dynamics in a hybrid fiber deliver an order of magnitude better noise performance than stand-alone ANDi fiber SC sources, which so far were considered the benchmark of low-noise SC generation. Our approach converts a standard ultrafast Er:fiber laser into an octave-spanning SC source with excellent phase coherence and lower RIN than could be previously obtained with any fiber-based SC source, and requiring less than 1/5th of the injected peak power that would be necessary to obtain equal spectral bandwidth in the stand-alone ANDi fiber. The fibers required to reproduce our experiments are commercially available from an online catalogue at a combined cost of US $50.

This advance is based on two important physical discoveries. First, we show through highly sensitive RIN measurements that the stability of ANDi SC sources is ultimately limited by the occurrence of PMI, even in commercial-grade, PANDA-style PM step-index designs pumped by 100 fs pulses. Second, we identify a noise suppression mechanism in the hybrid fiber, which is based on soliton compression strongly enhancing the subsequent OWB dynamics and, thus, preventing the accumulative buildup of PMI noise. This beneficial impact of hybrid fibers for the noise reduction of SC sources was previously not recognized.

We note that the hybrid scheme can be scaled for lasers with pulse repetition rates of hundreds of megahertz or gigahertz with limited peak power per pulse. The soliton compression factor and pulse quality solely depend on the soliton number N, and keeping $N \simeq 5$ typically yields a good compromise between the two factors [23]. Hence, by choosing a pre-compression fiber with suitable nonlinearity and dispersion, e.g., from the range of highly nonlinear fibers available from several manufacturers, a wide range of laser pulse peak powers and durations can be accommodated [50]. Similarly, choosing an ANDi fiber with dispersion closer to zero enhances the wave-breaking-dominated spectral broadening [51,52]. The low-noise nonlinear spectral broadening dynamics presented here are, thus, readily transferable to various laser platforms.

We anticipate this work to be particularly relevant for high-precision laser applications where intensity or phase-noise critically matter, including hyperspectral and multimodal imaging, frequency comb spectroscopy, synchronization of ultrafast light sources, arbitrary optical waveform generation, photonic radars, and photonic signal processing such as analog-to-digital converters, where peak-to-peak power fluctuations of <0.1% are required for achieving 10-bit resolution [31]. High amplitude stability also minimizes indirect system performance degradation by noise coupling processes, such as amplitude-to-phase noise conversion in photodiodes or intensity-to-f_{ceo} noise conversion in optical frequency combs [53,54].

Funding. Schweizerischer Nationalfonds zur Förderung der Wissenschaftlichen Forschung (PCEFP2_181222).

Disclosures. The authors declare no conflict of interest.

Data availability. Data underlying the results in this paper are openly available in [55].

Supplemental document. See Supplement 1 for supporting content.

REFERENCES

1. R. Alfano, ed., *The Supercontinuum Laser Source*, 3rd ed. (Springer, 2016).
2. T. Sylvestre, E. Genier, A. N. Ghosh, P. Bowen, G. Genty, J. Troles, A. Mussot, A. C. Peacock, M. Klimczak, A. M. Heidt, J. C. Travers, O. Bang, and J. M. Dudley, "Recent advances in supercontinuum generation in specialty optical fibers [invited]," J. Opt. Soc. Am. B **38**, F90–F103 (2021).
3. A. Rampur, D.-M. Spangenberg, B. G. A. Sierro, P. M. Hänzi, M. Klimczak, and A. Heidt, "Perspective on the next generation of ultra-low noise fiber supercontinuum sources and their emerging applications in spectroscopy, imaging, and ultrafast photonics," Appl. Phys. Lett. **118**, 240504 (2021).
4. D. M. Lesko, H. Timmers, S. Xing, A. Kowligy, A. J. Lind, and S. A. Diddams, "A six-octave optical frequency comb from a scalable few-cycle erbium fibre laser," Nat. Photonics **15**, 281–286 (2021).
5. U. Elu, L. Maidment, L. Vamos, F. Tani, D. Novoa, M. H. Frosz, V. Badikov, D. Badikov, V. Petrov, P. St.J. Russell, and J. Biegert, "Seven-octave high-brightness and carrier-envelope-phase-stable light source," Nat. Photonics **15**, 277–280 (2021).
6. L. Lundberg, M. Mazur, A. Mirani, B. Foo, J. Schröder, V. Torres-Company, M. Karlsson, and P. A. Andrekson, "Phase-coherent lightwave communications with frequency combs," Nat. Commun. **11**, 201 (2020).
7. C. Deakin and Z. Liu, "Dual frequency comb assisted analog-to-digital conversion," Opt. Lett. **45**, 173–176 (2020).
8. E. Temprana, E. Myslivets, B.-P. Kuo, L. Liu, V. Ataie, N. Alic, and S. Radic, "Overcoming Kerr-induced capacity limit in optical fiber transmission," Science **348**, 1445–1448 (2015).
9. J. M. Dudley, G. Genty, and S. Coen, "Supercontinuum generation in photonic crystal fiber," Rev. Mod. Phys. **78**, 1135–1184 (2006).
10. K. L. Corwin, N. R. Newbury, J. M. Dudley, S. Coen, S. A. Diddams, K. Weber, and R. S. Windeler, "Fundamental noise limitations to supercontinuum generation in microstructure fiber," Phys. Rev. Lett. **90**, 113904 (2003).
11. U. Møller and O. Bang, "Intensity noise in normal-pumped picosecond supercontinuum generation, where higher-order Raman lines cross into anomalous dispersion regime," Electron. Lett. **49**, 63–65 (2013).
12. S. Wabnitz, "Modulational polarization instability of light in a nonlinear birefringent dispersive medium," Phys. Rev. A **38**, 2018–2021 (1988).
13. I. B. Gonzalo, R. D. Engelsholm, M. P. Sørensen, and O. Bang, "Polarization noise places severe constraints on coherence of all-normal dispersion femtosecond supercontinuum generation," Sci. Rep. **8**, 6579 (2018).
14. A. M. Heidt, A. Hartung, and H. Bartelt, "Generation of ultrashort and coherent supercontinuum light pulses in all-normal dispersion fibers," in *The Supercontinuum Laser Source: The Ultimate White Light* (Springer, 2016), pp. 247–280.
15. P. Abdolghader, A. F. Pegoraro, N. Y. Joly, A. Ridsdale, R. Lausten, F. Légaré, and A. Stolow, "All normal dispersion nonlinear fibre supercontinuum source characterization and application in hyper-spectral stimulated Raman scattering microscopy," Opt. Express **28**, 35997–36008 (2020).
16. K. J. Kaltenecker, D. S. S. Rao, M. Rasmussen, H. B. Lassen, E. J. R. Kelleher, E. Krauss, B. Hecht, N. A. Mortensen, L. Gruener-Nielsen, C. Markos, O. Bang, N. Stenger, and P. U. Jepsen, "Near-infrared nanospectroscopy using a low-noise supercontinuum source," APL Photon. **6**, 066106 (2021).

17. S. Rao, M. Jensen, L. Grüner-Nielsen, J. T. Olsen, P. Heiduschka, B. Kemper, J. Schnekenburger, M. Glud, M. Mogensen, N. M. Israelsen, and O. Bang, "Shot-noise limited, supercontinuum-based optical coherence tomography," Light Sci. Appl. **10**, 133 (2020).
18. H. Tu, Y. Liu, D. Turchinovich, M. Marjanovic, J. K. Lyngsø, J. Lægsgaard, E. J. Chaney, Y. Zhao, S. You, W. L. Wilson, B. Xu, M. Dantus, and S. A. Boppart, "Stain-free histopathology by programmable supercontinuum pulses," Nat. Photonics **10**, 534–540 (2016).
19. K. P. Herdzik, K. N. Bourdakos, P. B. Johnson, A. P. Lister, A. P. Pitera, C.-Y. Guo, P. Horak, D. J. Richardson, J. H. Price, and S. Mahajan, "Multimodal spectral focusing CARS and SFG microscopy with a tailored coherent continuum from a microstructured fiber," Appl. Phys. B **126**, 84 (2020).
20. A. M. Heidt, J. M. Hodasi, A. Rampur, D.-M. Spangenberg, M. Ryser, M. Klimczak, and T. Feurer, "Low noise all-fiber amplification of a coherent supercontinuum at 2 μm and its limits imposed by polarization noise," Sci. Rep. **10**, 16734 (2020).
21. A. Rampur, Y. Stepanenko, G. Stepniewski, T. Kardas, D. Dobrakowski, D.-M. Spangenberg, T. Feurer, A. Heidt, and M. Klimczak, "Ultra low-noise coherent supercontinuum amplification and compression below 100 fs in an all-fiber polarization-maintaining thulium fiber amplifier," Opt. Express **27**, 35041–35051 (2019).
22. A. M. Heidt, J. S. Feehan, J. H. V. Price, and T. Feurer, "Limits of coherent supercontinuum generation in normal dispersion fibers," J. Opt. Soc. Am. B **34**, 764–775 (2017).
23. C.-M. Chen and P. L. Kelley, "Nonlinear pulse compression in optical fibers: scaling laws and numerical analysis," J. Opt. Soc. Am. B **19**, 1961–1967 (2002).
24. G. Genty, S. Coen, and J. M. Dudley, "Fiber supercontinuum sources (invited)," J. Opt. Soc. Am. B **24**, 1771–1785 (2007).
25. T. Hori, J. Takayanagi, N. Nishizawa, and T. Goto, "Flatly broadened, wideband and low noise supercontinuum generation in highly nonlinear hybrid fiber," Opt. Express **12**, 317–324 (2004).
26. P. Ciąćka, A. Rampur, A. Heidt, T. Feurer, and M. Klimczak, "Dispersion measurement of ultra-high numerical aperture fibers covering thulium, holmium, and erbium emission wavelengths," J. Opt. Soc. Am. B **35**, 1301–1307 (2018).
27. S. Preble, "UHNA fiber—efficient coupling to silicon waveguides," Nufern Application Note NuApp-3 (Coherent-Nufern, 2016).
28. D. Spangenberg, P. Neethling, E. Rohwer, M. H. Brügmann, and T. Feurer, "Time-domain ptychography," Phys. Rev. A **91**, 021803 (2015).
29. A. M. Heidt, D.-M. Spangenberg, M. Brügmann, E. G. Rohwer, and T. Feurer, "Improved retrieval of complex supercontinuum pulses from XFROG traces using a ptychographic algorithm," Opt. Lett. **41**, 4903–4906 (2016).
30. R. P. Scott, C. Langrock, and B. H. Kolner, "High-dynamic-range laser amplitude and phase noise measurement techniques," IEEE J. Sel. Top. Quantum Electron. **7**, 641–655 (2001).
31. J. Kim and Y. Song, "Ultralow-noise mode-locked fiber lasers and frequency combs: principles, status, and applications," Adv. Opt. Photon. **8**, 465–540 (2016).
32. A. Rampur, D.-M. Spangenberg, G. Stepniewski, D. Dobrakowski, K. Tarnowski, K. Stefanska, A. Pazdzior, P. Mergo, T. Martynkien, T. Feurer, M. Klimczak, and A. M. Heidt, "Temporal fine structure of all-normal dispersion fiber supercontinuum pulses caused by non-ideal pump pulse shapes," Opt. Express **28**, 16579–16593 (2020).
33. A. Klose, G. Ycas, D. L. Maser, and S. A. Diddams, "Tunable, stable source of femtosecond pulses near 2 μm via supercontinuum of an erbium mode-locked laser," Opt. Express **22**, 28400–28411 (2014).
34. M. Klimczak, G. Soboń, R. Kasztelanic, K. M. Abramski, and R. Buczyński, "Direct comparison of shot-to-shot noise performance of all normal dispersion and anomalous dispersion supercontinuum pumped with sub-picosecond pulse fiber-based laser," Sci. Rep. **6**, 19284 (2016).
35. B. Sierro and A. M. Heidt, "Noise amplification in all-normal dispersion fiber supercontinuum generation and its impact on ultrafast photonics applications," OSA Contin. **3**, 2347–2361 (2020).
36. E. Genier, S. Grelet, R. D. Engelsholm, P. Bowen, P. M. Moselund, O. Bang, J. M. Dudley, and T. Sylvestre, "An ultra-flat, low-noise, and linearly polarized fiber supercontinuum source covering 670–1390 nm," Opt. Lett. **46**, 1820–1823 (2021).
37. B. Resan, S. Kurmulis, V. Markovic, and K. J. Weingarten, "1% rms amplitude noise from a 30 fs continuum based source tunable from 800 to 1250 nm," Opt. Express **24**, 14960–14965 (2016).
38. D. S. S. Rao, R. D. Engelsholm, I. B. Gonzalo, B. Zhou, P. Bowen, P. M. Moselund, O. Bang, and M. Bache, "Ultra-low-noise supercontinuum generation with a flat near-zero normal dispersion fiber," Opt. Lett. **44**, 2216–2219 (2019).
39. G. Agrawal, *Nonlinear Fiber Optics* (Academic, 2007).
40. F. Poletti and P. Horak, "Description of ultrashort pulse propagation in multimode optical fibers," J. Opt. Soc. Am. B **25**, 1645–1654 (2008).
41. J. W. Nicholson and M. F. Yan, "Cross-coherence measurements of supercontina generated in highly-nonlinear, dispersion shifted fiber at 1550 nm," Opt. Express **12**, 679–688 (2004).
42. X. Gu, M. Kimmel, A. Shreenath, R. Trebino, J. Dudley, S. Coen, and R. Windeler, "Experimental studies of the coherence of microstructure-fiber supercontinuum," Opt. Express **11**, 2697–2703 (2003).
43. D. Türke, S. Pricking, A. Husakou, J. Teipel, J. Herrmann, and H. Giessen, "Coherence of subsequent supercontinuum pulses generated in tapered fibers in the femtosecond regime," Opt. Express **15**, 2732–2741 (2007).
44. N. Nishizawa and J. Takayanagi, "Octave spanning high-quality supercontinuum generation in all-fiber system," J. Opt. Soc. Am. B **24**, 1786–1792 (2007).
45. N. Singh, M. Xin, D. Vermeulen, K. Shtyrkova, N. Li, P. T. Callahan, E. S. Magden, A. Ruocco, N. Fahrenkopf, C. Baiocco, B. P.-P. Kuo, S. Radic, E. Ippen, F. X. Kärtner, and M. R. Watts, "Octave-spanning coherent supercontinuum generation in silicon on insulator from 1.06 μm to beyond 2.4 μm," Light Sci. Appl. **7**, 17131 (2018).
46. A. R. Johnson, A. S. Mayer, A. Klenner, K. Luke, E. S. Lamb, M. R. E. Lamont, C. Joshi, Y. Okawachi, F. W. Wise, M. Lipson, U. Keller, and A. L. Gaeta, "Octave-spanning coherent supercontinuum generation in a silicon nitride waveguide," Opt. Lett. **40**, 5117–5120 (2015).
47. M. Närhi, J. Turunen, A. T. Friberg, and G. Genty, "Experimental measurement of the second-order coherence of supercontinuum," Phys. Rev. Lett. **116**, 243901 (2016).
48. K. Tarnowski, T. Martynkien, P. Mergo, J. Sotor, and G. Soboń, "Compact all-fiber source of coherent linearly polarized octave-spanning supercontinuum based on normal dispersion silica fiber," Sci. Rep. **9**, 12313 (2019).
49. J. W. Nicholson, A. D. Yablon, M. F. Yan, P. Wisk, R. Bise, D. J. Trevor, J. Alonzo, T. Stockert, J. Fleming, E. Monberg, F. Dimarcello, and J. Fini, "Coherence of supercontinua generated by ultrashort pulses compressed in optical fibers," Opt. Lett. **33**, 2038–2040 (2008).
50. D. Brida, G. Krauss, A. Sell, and A. Leitenstorfer, "Ultrabroadband Er:fiber lasers," Laser Photon. Rev. **8**, 409–428 (2014).
51. A. M. Heidt, "Pulse preserving flat-top supercontinuum generation in all-normal dispersion photonic crystal fibers," J. Opt. Soc. Am. B **27**, 550–559 (2010).
52. K. Tarnowski, T. Martynkien, P. Mergo, K. Poturaj, A. Anuszkiewicz, P. Béjot, F. Billard, O. Faucher, B. Kibler, and W. Urbanczyk, "Polarized all-normal dispersion supercontinuum reaching 2.5 μm generated in a birefringent microstructured silica fiber," Opt. Express **25**, 27452–27463 (2017).
53. E. Ivanov, S. Diddams, and L. Hollberg, "Study of the excess noise associated with demodulation of ultra-short infrared pulses," IEEE Trans. Ultrason. Ferroelectr. Freq. Control **52**, 1068–1074 (2005).
54. N. Newbury and B. Washburn, "Theory of the frequency comb output from a femtosecond fiber laser," IEEE J. Quantum Electron. **41**, 1388–1402 (2005).
55. , "B. Sierro, P. Hänzi, D. Spangenberg, A. Rampur, and A. M. HeidtDataset: Reducing the noise of fiber supercontinuum sources to its limits by exploiting cascaded soliton and wave breaking nonlinear dynamics," Bern Open Repository and Information System (BORIS) (2022), https://doi.org/10.48620/41.